

Tensor Processing Primitives: A Programming Abstraction for Efficiency and Portability in Deep Learning Workloads

Evangelos Georganas*, Dhiraj Kalamkar*, Sasikanth Avancha*, Menachem Adelman*, Cristina Anderson*, Alexander Breuer[#], Narendra Chaudhary*, Abhisek Kundu*, Vasimuddin Md*, Sanchit Misra*, Ramanarayan Mohanty*, Hans Pabst*, Barukh Ziv*, Alexander Heinecke*

*Intel Corporation

[#]Friedrich-Schiller-Universität Jena

ABSTRACT

During the past decade, novel Deep Learning (DL) algorithms/workloads and hardware have been developed to tackle a wide range of problems. Despite the advances in workload/hardware ecosystems, the programming methodology of DL-systems is stagnant. DL-workloads leverage either highly-optimized, yet platform-specific and inflexible kernels from DL-libraries, or in the case of novel operators, reference implementations are built via DL-framework primitives with underwhelming performance. This work introduces the Tensor Processing Primitives (TPP), a programming abstraction striving for efficient, portable implementation of DL-workloads with high-productivity. TPPs define a compact, yet versatile set of 2D-tensor operators (or a virtual Tensor ISA), which subsequently can be utilized as building-blocks to construct complex operators on high-dimensional tensors. The TPP specification is platform-agnostic, thus code expressed via TPPs is portable, whereas the TPP implementation is highly-optimized and platform-specific. We demonstrate the efficacy of our approach using standalone kernels and end-to-end DL-workloads expressed entirely via TPPs that outperform state-of-the-art implementations on multiple platforms.

1 INTRODUCTION

Since the advent of Deep Learning (DL) as one of the most promising machine learning paradigms almost 10 years ago, deep neural networks have advanced the fields of computer vision, natural language processing, recommender systems, and gradually pervade an increasing number of scientific domains [1–10]. Due to the diverse nature of the problems under consideration, these DL workloads exhibit a wide range of computational characteristics and demands. Furthermore, due to the immense computational cost of such workloads, industry and academia have developed specialized hardware features on commodity processors, and even specialized accelerators in order to harness these computational needs [11].

In contrary to the fast-evolving ecosystems of DL workloads and DL-oriented hardware/accelerators, the programming paradigm of DL systems has reached a plateau [12]. More specifically, the development of novel DL workloads involves two types of components: i) Well-established operators within DL libraries (e.g. 2D convolutions, inner-product, batch-norm layers in oneDNN [13] and cuDNN [14]), and ii) Unprecedented, custom primitives which typically instantiate new algorithmic concepts/computational motifs. Unfortunately both of these components come with their shortcomings.

On one hand, the operators within DL libraries are heavily optimized and tuned (usually by vendors) in a platform-specific fashion,

leading to monolithic, non-portable and inflexible kernels. Additionally, such opaque and high-level operators prohibit modular design choices since the user/frameworks have to adhere to particular interfaces that may not be adapted to fit the operation under consideration. On the other hand, the custom/unprecedented primitives are typically implemented by the user via the available generic/reference primitives of an ML framework which are not optimized and as such yield underwhelming performance. It is up to the user to create optimized implementations for the custom primitives, leading again to code which is non-portable and potentially requires hardware expertise in order to achieve peak performance. Unfortunately, most of the times such expertise is not available to the data/ML scientist who is developing the custom DL primitive. Therefore, the deployment (or even the evaluation) of a new operator typically requires yet another stage in the development cycle where low-level optimization experts are working on the re-write/fine-tuning of the operator. Later on, in case an operator proves to be important for the community, systems researchers and vendors standardize it, and potentially create yet another monolithic kernel within a DL library for further re-use within DL frameworks. This entire development cycle potentially takes a considerable amount of time (up to years in some cases) and inadvertently impedes the efficient exploration of innovative machine learning ideas [12]. An alternative approach to optimize both types of operators is to leverage contemporary Tensor Compilers (e.g. [15–18]), however the state-of-the-art tools are only suitable for compiling small code-blocks whereas large-scale operators require prohibitive compilation times, and often the resulting code is far from the achievable peak [12].

We identify that the common source of the problems mentioned in the previous paragraph is the extreme levels of abstraction offered by the DL libraries and the Tensor Compilers. The DL libraries offer coarse-grain, monolithic and inflexible operators whereas the Tensor Compilers usually go to the other extreme, allowing the user to express arbitrary low-level operators without any minimal restrictions that would readily enable efficient lifting and code-generation in their back-ends (e.g. they offer no minimal/compact set of allowed operations on tensors). To exacerbate the challenge of optimal code generation, Tensor Compilers usually undertake the cumbersome tasks of efficient parallelization, loop re-orderings, automatic tiling and layout transformations, which, to date, remain unsolved in the general setup. Also, there is not a well-established way to share state-of-the-art optimizations among the plethora of Tensor Compilers and as a result each one has its own advantages and disadvantages, which translates eventually to sub-optimal performance on real-world scenarios [19]. We note here the recent,

promising effort of MLIR [20] towards unifying the optimization efforts in the Tensor Compiler IR infrastructure.

In this work we introduce the Tensor Processing Primitives (TPP), a programming abstraction striving for efficient and portable implementation of Tensor operations, with a special focus on DL workloads. TPPs define a set of relatively low-level primitive operators on 2D Tensors, which in turn can be used as basic building blocks to construct more complex operators on high-dimensional tensors. TPPs comprise a minimal and compact, yet expressive set of precision-aware, 2D tensor level operators to which high-level DL operators can be reduced. TPPs’s specification is agnostic to targeted platform, DL framework, and compiler back-end. As such the code which is expressed in terms of TPPs is portable. Since the level of abstraction that TPPs adopt is at the sub-tensor granularity, TPPs can be directly employed by DL workload developers within the frameworks, or could be alternatively used to back up an IR within a Tensor Compiler stack, i.e. TPPs could form the basis of an MLIR dialect.

While the TPP specification is agnostic of the targeted framework/platform/compiler stack, its implementation is platform specific, and is optimized for the target architectures. This subtle detail offers a clear separation of concerns: the user-entity of TPPs, either a developer or a compiler framework, can focus on expressing the desired algorithm and its execution schedule (e.g. parallelization, loop orders) using the TPP tensor abstraction, whereas the efficient, platform-specific code generation pertaining to the TPP operations belongs to the TPP back-end. To this extent, TPPs could be also viewed as a “virtual Tensor ISA” that abstracts the actual physical ISA of the target (e.g. SSE, AVX2, AVX512, AMX for x86, AArch64 and ARMv8 SVE , xPU). In our Proof-Of-Concept (POC) implementation of TPPs we leverage JIT technology to emit performant and platform-specific code during runtime. Furthermore, in our POC we define a mini embedded Domain Specific Language (mini-eDSL) where the TPPs can be combined via matrix equations in order to build high-level operators without sacrificing performance.

We demonstrate the efficiency of our approach on multiple platforms using standalone kernels written entirely with TPPs and compare the performance to vectorized-by-expert code and compiler generated code. Finally, we showcase the expressiveness and viability of our methodology by implementing contemporary end-to-end DL workloads using solely the TPP abstractions and show how we can outperform the state-of-the-art implementations on multiple platforms. The main contributions of this work are:

- A TPP specification/foundation for primitive tensor operations.
- A Proof-Of-Concept implementation of the TPP specification along with a mini-eDSL, enabling efficient fusion of TPPs that lead to efficient, portable high-level tensor operations.
- A demonstration of how contemporary and novel DL algorithmic motifs/workloads can be expressed in their entirety via TPPs.
- An experimental evaluation of the TPP-based DL workloads from all relevant fields (image processing, recommendation systems, natural language processing, graph processing and applications in science) on multiple platforms (different instruction set architectures (ISAs) x86_64 and aarch64, and micro-architectures for

each ISA), including distributed-memory scaling. We show performance that matches/exceeds the state-of-the-art implementations, while maintaining flexibility, portability and obviating the need for low-level platform-specific optimizations.

Section 2 details the specification of the TPPs. Then, Section 3 illustrates a POC implementation of the TPP specification along with an infrastructure that enables efficient TPP fusion. In Section 4 we exhibit how contemporary DL motifs/algorithmic paradigms can be expressed via TPPs. Section 5 presents an experimental evaluation of TPP-based DL kernels and workloads on multiple platforms. Sections 6 and 7 summarize the related work and conclude this paper.

2 THE TPP SPECIFICATION

2.1 TPP Design Principles

The TPP specification is driven by a few design principles:

1) *Each TPP corresponds to a mathematical operator that takes a number of input(s) and produces an output.* We opt to specify TPPs that correspond to basic, well-defined mathematical tensor operations. In this way we keep the set of TPPs *minimal* albeit *expressive*; basic TPPs can be combined to formulate more complex operators.

2) *The inputs/outputs of the TPPs are abstract 2D tensors that can be fully specified by their shape/size, leading dimensions, and precision.* Additionally, the 2D tensors hold the following complementary *runtime* information: (i) a *primary* field which corresponds to the memory address where the 2D (sub)tensor data resides, (ii) a *secondary* field holding optional data for the tensor (e.g. a mask for the tensor), and (iii) a *tertiary* field holding optional, auxiliary information of the tensor, (e.g. scaling factors for a quantized tensor.)

3) *TPPs are specified as “memory-to-memory” operations, or equivalently the input/output tensors are residing in memory locations specified by the user.* This design decision is critical in order to abstract the TPPs from all physical ISAs, and enables true platform-agnostic specification.

4) *TPPs have declarative semantics.* As such, the TPP specification does not preclude potential parallelism (e.g. SIMD, SIMT) in the back-end implementation which is target-specific.

5) *TPPs are composable in a producer-consumer fashion.* Since the output of a TPP is a well-defined tensor O_i , it can be fed as input to a subsequent TPP. In such a scenario, this “intermediate” tensor O_i is not necessarily exposed to the user, unless the user explicitly requires it (e.g. by combining the TPPs in a manual fashion via an explicit temporary O_i buffer/tensor which lives in the user space/application). This flexibility allows the TPP implementation (which is platform-specific) to combine TPPs in the most efficient way for the target architecture (e.g. the O_i tensor can live at the physical register file in the composite TPP in order to avoid redundant memory movement).

6) *The TPP input/output tensors as well as the computation itself are precision aware.* This feature makes mixed precision computations (that are prominent in DL workloads) easy to express from the user point of view, and provides information to the TPP back-end that may enable efficient implementation.

Unary TPP	Description/Comments
Identity	Copies input to output. Given input/output datatype, it performs datatype conversions
Zero	Fills output with zeros
Square	Squares input and stores to output
Increment / decrement	Increments / Decrements input by 1 and stores to output
Square root	Computes the square root of input and stores to output
Reciprocal	Computes the reciprocal of input and stores to output
Rcp. Sqrt.	Computes the rcp. sqrt. of input and stores to output
Exp	Computes the exponential value of the input tensor entries and stores them to output
PRNG	Generates an output tensor with pseudo-random entries
(De)Quantize	Quantizes / Dequantizes the input
Reduce	Reduces the rows/columns of the input and stores to output. The reduction function can be SUM/MUL/MIN/MAX; (optionally) reduces the <i>squared</i> input
Transform	Transforms input and stores to output. Transformations are: Transpose, VNNI formatting, and VNNI to VNNI-transpose
Unpack	Takes each entry $x_{i,j}$ of the input tensor, splits it in two parts $x_{i,j}^{lo}$ and $x_{i,j}^{hi}$ with same bit-width, and stores them in two tensors X^{lo}, X^{hi}
Replicate columns	Takes an input column/vector, replicates it a variable number of times and forms the output
Gather / Scatter	Gathers/Scatters rows/columns from input and forms the tensor
2D Gat./Sca.	Gathers/scatters elements from input using 2D offsets
2D-strided loads/stores	Loads/stores elements from/to a tensor using primary and secondary strides
Tanh & Tanh_inv	Computes the hyperbolic tangent function (or its inv used for back-propagation) on input
RELU & RELU_inv	Apply a Rectified Linear Unit function (or its inv used for back-propagation) on input
Sigmoid & Sigmoid_inv	Computes the logistic sigmoid (or its inv used for back-propagation) on input
GELU & GELU_inv	Apply a Gaussian Error Linear Unit function (or its inv used for back-propagation) on input
Dropout & Dropout_inv	Drops out values from the input tensor with probability p . For the inv/back-propagation pass, the same dropped units are zeroed out

Table 1: Unary TPPs

2.2 TPP Arguments

As mentioned in the previous subsection, the input to TPPs are 2D tensors. Each 2D tensor can be specified by the number of rows M , columns N , its leading dimension ld and its datatype $dtype$. Additionally, during runtime each tensor gets fully characterized by specifying its location/address as *primary* info, optional companion tensor info as *secondary* (e.g. sparsity bitmask), and optionally *tertiary* info (e.g. in case the tensor shape is dynamically determined at runtime, this info may contain variables specifying M/N). Each TPP also specifies the shape/precision of the produced/output 2D tensor

Each TPP also supports input tensors with *broadcast* semantics. More specifically, TPPs accept optional flags dictating that the input 2D tensor should be formed by broadcasting a column/row/scalar $N/M/M \times N$ times respectively. Finally, the TPPs accept optional flags which further specify the TPP operation. For example, in case a TPP is computing a transcendental function, the flags may be specifying various approximation algorithms used for the computation. In the next subsection we present the TPPs in three groups: *unary*, *binary*, and *ternary* TPPs given the number of input tensors they accept.

Binary TPP	Description/Comments
Add	Add two inputs
Sub	Subtracts two inputs
Mul	Multiplies (elementwise) two inputs
Div	Divides two inputs
Max/Min	Finds element-wise max/min of two inputs
MatMul	Performs matrix multiplication of two input
Pack	Concatenates pairs of entries $x_{i,j}^{lo}$ and $x_{i,j}^{hi}$ from the inputs X^{lo}, X^{hi} to $x_{i,j}$ and stores it to the output X
Compare	Compares element-wise two inputs and stores a bitmask of the comparison

Table 2: Binary TPPs

Ternary TPP	Description/Comments
GEMM	Performs on 2D inputs A, B, C , scalar β : $C = \beta C + A \times B$
Batch-Reduce GEMM	Performs on 2D inputs A_i, B_i (with $i = 0, 1, \dots, n-1$), C , scalar β : $C = \beta C + \sum_{i=0}^{n-1} A_i \times B_i$
(N)MulAdd	Performs on 2D inputs A, B, C : $C = C + A \odot B$ (or $C = C - A \odot B$); \odot denotes element-wise multiplication
Blend	blends 2D input tensors A, B according to bitmask C

Table 3: Ternary TPPs

2.3 The TPP collection

First, we highlight the ternary *Batch-Reduce GEMM* (BRGEMM) TPP which is the main building block for general tensor contractions in DL kernels [21]. BRGEMM materializes the operation $C = \beta \cdot C + \sum_{i=0}^{n-1} A_i \times B_i$. In essence, this kernel multiplies the specified blocks $A_i^{M \times K}$ and $B_i^{K \times N}$ and reduces the partial results to a block $C^{M \times N}$. It is noteworthy that tensors A and B can alias and also the blocks A_i and B_i can reside in any position in the input (potentially high-dimensional) tensors A and B . Previous work [21] has shown that this single building block is sufficient to express efficiently tensor contractions in the most prevalent DL computational motifs, namely: Convolution Neural Networks (CNN), Fully-Connected networks (FC), Multi-Layer Perceptrons (MLP), Recurrent Neural Networks (RNN)/Long Short-Term Memory (LSTM) Networks. In Section 4 we exhibit how BRGEMM can be further used to build efficient Attention Cells that comprise the cornerstone of modern Natural Language Processing (NLP) workloads. BRGEMM can be specialized to one of the following three variants that may enable more efficient implementations on various platforms: (i) *address-based BRGEMM*, where the addresses of the blocks A_i and B_i are explicitly provided by the user, (ii) *offset-based BRGEMM*, where the addresses of A_i and B_i can be computed as $address_A_i = address_A + offset_{A_i}$ and $address_B_i = address_B + offset_{B_i}$, and (iii) *stride-based BRGEMM*, where the addresses of A_i and B_i are: $address_A_i = address_A_{i-1} + stride_A$ and $address_B_i = address_B_{i-1} + stride_B$.

Table 1 presents the unary TPPs that accept one 2D tensor as input. Since most of these TPPs map directly to the equivalent math function, we further elaborate only on the ones which are more complex. The *Identity* TPP essentially copies the input to the output. Since the input and output are fully specified in terms of their precision, this TPP can be also used to perform datatype conversions between tensors.

The *Quantize & Dequantize* TPPs are used to quantize/dequantize the input tensor whereas the exact algorithm employed is specified by a TPP flag.

The *Transform* TPP uses a flag to determine the exact transformation applied on the input 2D tensor. The *Transpose* transformation is the usual mathematical matrix transpose. The rest two types of transformation, namely *VNNI formatting*, and *VNNI to VNNI-transpose* are DL specific. More specifically, modern hardware (e.g. Intel’s Cooper Lake) requires tensors to be in specific format called *VNNI* in order to employ hardware acceleration for specific operations (e.g. dot-products). This format represents a logical 2D tensor $[D_1][D_0]$ as a 3D tensor $[D_1/\alpha][D_0][\alpha]$ where essentially the dimension D_1 is blocked in chunks of size α , which in turn are set as the inner-most tensor dimension. The *VNNI formatting* TPP performs this exact transformation: $[D_1][D_0] \rightarrow [D_1/\alpha][D_0][\alpha]$ and the *VNNI to VNNI-transpose* transposes a tensor which is already laid out in VNNI format, i.e. performs $[D_1/\alpha][D_0][\alpha] \rightarrow [D_0/\alpha_0][D_1][\alpha_0]$.

The last four entries of Table 1 correspond to DL-specific operations. They correspond to activation functions typically encountered in DL workloads. All these activation functions have a counterpart which is required during the back-propagation pass of training DL networks. These DL specific TPPs could be built on top of other TPPs, however since they are prevalent in DL workloads we opt to define them as self-contained TPPs for ease of usage. Table 2 and Table 3 present the binary/ternary TPPs that accept two/three 2D tensor as inputs respectively.

3 TPP IMPLEMENTATION

In this Section we briefly describe our Proof-Of-Concept implementation of the TPP specification. Our implementation targets multiple CPU architectures from various vendors that support different ISAs, but could be readily extended to support even GPU ISAs. We build upon and extend the open source LIBXSMM [22] library which leverages JIT techniques. Such JIT techniques have been successfully used for optimal code generation on CPUs by taking advantage of the known (at runtime) tensor shapes/dimensions in HPC and DL applications [21–23]. Nevertheless, the TPP specification is platform-agnostic and does not preclude any TPP back-end implementation.

3.1 Generic TPP Structure

Algorithm 1 exhibits at a high-level the pseudocode that is used to implement the Unary/Binary/Ternary TPPs in a unified fashion. The inputs of the TPPs are tensors X, Y (in case of binary/ternary TPPs) and Z (in case of ternary TPP), and an output tensor O . For the purposes of this simplified presentation we assume all tensors are of size $M \times N$, however, depending on the operation these might have different sizes. For example, if the unary OP is a reduction-by-columns and the input is $M \times N$, then the output is an $M \times 1$ vector. First, we show that the M/N loops are blocked with factors m_b/n_b such that the working sets of each microkernels fits on the available register file. The latter is architecture specific, e.g. AVX2-enabled ISAs expose 16 256-bit vector registers, AVX512-enabled ISAs expose 32 512-bit vector registers and Aarch64 features 32 128-bit (NEON)/512-bit (SVE) vector registers. The “load_generic” function

Algorithm 1 The generic unary/binary/ternary TPP algorithm

Inputs: $X^{M \times N}, (Y^{M \times N}, Z^{M \times N})$ if binary/ternary

Output: $O^{M \times N}$

```

1: for  $i_n = 0 \dots N - 1$  with step  $n_b$  do
2:   for  $i_m = 0 \dots M - 1$  with step  $m_b$  do
3:      $\triangleright$  Generic loads, may have broadcast/gather semantics,
4:      $\triangleright$  and may perform datatype conversions
5:      $X_b \leftarrow \text{load\_generic } m_b \times n_b \text{ X-subblock}_{i_m, i_n}$ 
6:     if (unary TPP) then
7:        $X_b \leftarrow \text{Unary\_op}(X_b)$ 
8:     if (binary TPP) then
9:        $Y_b \leftarrow \text{load\_generic } m_b \times n_b \text{ Y-subblock}_{i_m, i_n}$ 
10:       $X_b \leftarrow \text{Binary\_op}(X_b, Y_b)$ 
11:    if (ternary TPP) then
12:       $Y_b \leftarrow \text{load\_generic } m_b \times n_b \text{ Y-subblock}_{i_m, i_n}$ 
13:       $Z_b \leftarrow \text{load\_generic } m_b \times n_b \text{ Z-subblock}_{i_m, i_n}$ 
14:       $X_b \leftarrow \text{Ternary\_op}(X_b, Y_b, Z_b)$ 
15:     $\triangleright$  Generic store, may have scatter semantics, and may
16:     $\triangleright$  perform datatype conversion
17:     $O\text{-subblock}_{i_m, i_n} \xleftarrow{\text{store\_generic}} X_b$ 
```

used in Algorithm 1 denotes the loading of a sub-tensor to a register block; this load may imply row/column/scalar broadcast semantics if the user specified the TPP in that way, or even may have strided-load/gather semantics if the TPP involves a strided-load/gather operation. Also, for simplicity we do not show here the handling of “secondary” fields of the tensors that may be required (e.g. indices array for the gather operation, bitmasks arrays). Additionally, the generic load also handles datatype conversion, for instance provided the input is in bfloat16 (BF16) [24] whereas the compute is going to happen in FP32 precision. Once all the required sub-tensors are loaded, then the corresponding Unary/Binary/Ternary operator is applied. This operator may be directly mapped to an available instruction (e.g. a vector add in case of binary addition), or to a sequence of instructions for more complicated operators (e.g. reductions, random number generation via xorshift algorithm [25], approximation algorithms for transcendental functions [26]). Last but not least, the optimal sequence generation depends on the available instructions and this is handled by the TPP back-end/JITer. For example, some ISAs may have masking/predicate support (e.g. AVX512 & SVE) that enable efficient handling of loop remainders, the selected unrolling degree heavily depends on the instructions in use, their latency and the number of available architectural registers. Once the result is computed, the resulting register block is stored back to the corresponding output sub-tensor position. Similarly to the generic load, the “generic” store may induce strided accesses or may be even a scatter operation. Additionally, the generic store also handles potential datatype conversions.

3.2 BRGEMM TPP Structure

We present in more detail the BRGEMM TPP because it comprises the tensor contraction tool in the TPP abstraction, and is ubiquitous in the DL kernels and workloads described in Section 4. Algorithm 2 exhibits the high-level algorithm implementing: $C = \beta \cdot C + \sum_{i=0}^{n-1} A_i \times B_i$. Lines 1-2 block the computation of the result

Algorithm 2 The batch-reduce GEMM TPP

Inputs: $A_i^{M \times K}, B_i^{K \times N}$ for $i = 0, \dots, n-1$, $C^{M \times N}$, $\beta \in \mathbb{R}$
Output: $C = \beta \cdot C + \sum_{i=0}^{n-1} A_i \times B_i$

```

1: for  $i_n = 0 \dots N-1$  with step  $n_b$  do
2:   for  $i_m = 0 \dots M-1$  with step  $m_b$  do
3:      $\text{acc\_regs} \leftarrow \text{load\_generic } m_b \times n_b \text{ C-subblock}_{i_m, i_n}$ 
4:     for  $i = 0 \dots n-1$  with step 1 do
5:       for  $i_k = 0 \dots K-1$  with step  $k_b$  do
6:          $\triangleright$  Outer product GEMM microkernel
7:          $\text{acc\_regs} += A_i \text{ sub-panel}_{i_m, i_k} \times B_i \text{ sub-panel}_{i_k, i_n}$ 
8:        $\text{C-subblock}_{i_m, i_n} \xleftarrow{\text{store\_generic}} \text{acc\_regs}$ 
```

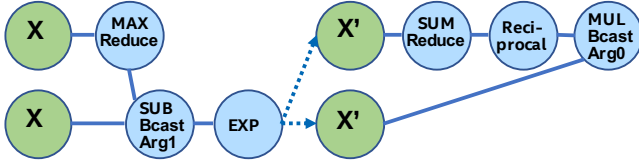


Figure 1: Softmax operator by combining TPPs.

C in $m_b \times n_b$ tensor sub-blocks. Once such a subblock is loaded into the accumulation registers (line 3), we loop over all pairs A_i, B_i (line 4) and we accumulate into the loaded registers the products of the corresponding $m_b \times K$ subblocks of A_i with the relevant $K \times n_b$ sub-blocks of B_i (lines 5-7). In order to calculate a partial product of an $m_b \times k_b$ sub-panel of A_i with a $k_b \times n_b$ sub-panel of B_i , we follow an outer product formulation. The loading of A_i and B_i sub-panels, and the outer-product formulation is heavily dependent on the target platform. We provide BRGEMM implementations for multiple x86 ISAs: SSE, AVX, AVX2, AVX512, including the recently introduced Intel AMX (Advanced Matrix Extensions) ISA [27]. Additionally, we have implemented the BRGEMM TPP for AArch64 and ARMv8 SVE ISAs. Depending on the targeted platform, the “register” can be either a typical vector register with varying width (e.g. 128-512bit vector length), or in the case of AMX-enabled target the “register” is a 2D tile-register. Similarly, the outer-product formulation may employ the available Fused-Multiply-Add (FMA) instructions, or even 2D tile-multiplication instructions. In all these cases, the TPP implementation emits the appropriate load/store/prefetch/FMA instructions, and takes into account the available architectural registers/unrolling factors/instruction mix in order to achieve close to peak performance. Last but not least, the BRGEMM supports multiple datatypes (FP64, FP32, BF16, INT8), and whenever possible employs hardware acceleration, e.g. via specialized FMA instructions for INT8/BF16 datatypes.

3.3 Combining TPPs via Matrix Equations

One of the main design principles of TPPs (as described in Section 2.1) is that they can be composed in a producer-consumer fashion to form complex operations. For example consider the scenario where a user wants to implement the composite operation $C = \text{Tanh}(A + B)$. One way to express this via TPPs would be to allocate an intermediate tensor tmp with same shape as A and B , and perform first $tmp = \text{Add}(A, B)$ via the binary Add TPP. Then

the user can compute the final result by leveraging the Tanh Unary TPP: $C = \text{Tanh}(tmp)$. Even though this approach is functionally correct, it requires the explicit management of intermediate tensors/buffers by the user and also may result in low performance since there are redundant loads/stores to the tmp tensor.

In order to increase the productivity, efficiency and expressiveness pertaining to composite operators, we implemented an embedded Domain Specific Language (eDSL) in LIBXSMM [22]. Our Proof-Of-Concept implementations allows the user to express the desired composite operator as a Matrix Equation. More specifically, the user can express the composite operator as an equation tree, where the head and internal nodes are the available TPPs, whereas the leaves of the trees are the input 2D tensors of the composite operation. Our code-gen parses the provided equation and emits/JITs a function implementing the desired operation. Figure 1 illustrates two Matrix Equation trees that are used to express the softmax operator [28] (see Section 4.1 for details):

$$Y = \text{softmax}(X) \text{ with } y_{ij} = \frac{e^{(x_{ij} - \max_{x_{ij} \in X} x_{ij})}}{\sum_{x_{ij} \in X} e^{(x_{ij} - \max_{x_{ij} \in X} x_{ij})}} \quad (1)$$

The eDSL back-end performs multiple analyses and optimizations passes. The input equation tree is analyzed, and TPP fusion opportunities are identified. Then, a secondary analysis is performed to minimize the intermediate tensor storage requirements and to increase the register reuse when passing/communicating results across the equation’s TPPs. This analysis performs an adaptive post-order traversal of the equation tree, where the computation (if possible) is performed to smaller sub-tensors that can fit in the available register file. The reuse/recycling among register blocks in this adaptive post-order evaluation is provably optimal and necessitated to maximize the register file reuse [29].

We want to highlight two aspects of the matrix equation JIT strategy that are essential for high performance and usability. First, when combining specific operations which exhibit *both* high register pressure and reuse (e.g. transposes, GEMM/BRGEMM, transcendental approximations), we decide to propagate the results towards the rest of the TPPs in the tree via stack-allocated temporal tensors. This design decision is done in order to avoid excessive register spills/reloads for such operations, since fusing vertically in the tree across multiple TPPs merely increases the register pressure, and it would diminish the benefits or register reuse within these operations. This stack-allocated tensor management is done automatically by the back-end and is transparent to the user. Second, in the back-end we identify idioms/motifs of combined TPPs (e.g. a gather TPP followed by a reduce TPP) and we can JIT an instruction sequence which is optimal for the composite access pattern.

Even though we developed a rudimentary method/POC of combining the TPPs via Matrix Equation Trees, we have found that it is sufficient to express all the complex operators we encountered in a wide-range of workloads discussed further in Section 4. Nevertheless, we envision that when/if TPPs are widely adopted within Tensor Compiler frameworks (e.g. as an MLIR dialect) then more complicated Graphs (instead of simple trees) and more sophisticated analyses/optimization passes can be leveraged during the composition of TPPs. The key-ingredient that makes the composition of

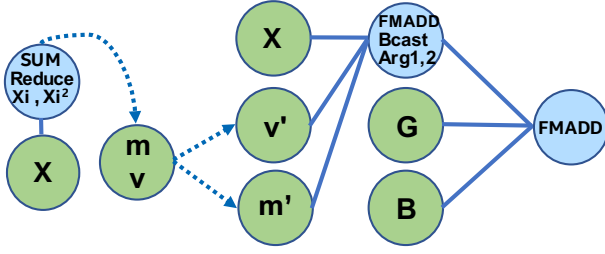


Figure 2: Layernorm via TPPs.

TPPs amenable to optimization opportunities is the TPP specification itself: TPPs comprise a small, well-defined compact set of tensor operators with declarative semantics as shown in Section 2.

4 TPP-BASED KERNELS & WORKLOADS

This section covers how DL kernels and workloads (image processing, recommendation systems, natural language processing, graph processing and applications in science) can leverage TPPs to achieve high performance. Although this paper’s work is targeting CPUs, we cover the entire training pipeline and not only inference. The main purpose of this is to demonstrate the versatility of TPPs which is valuable in the more complicated backward pass kernels, and to handle training’s implications to the forward pass.

4.1 Softmax Kernel

Equation 1 shows the formula for the softmax operator [28], which is often used as the last activation function of a neural network, aiming to normalize its output to a probability distribution. We can represent this operator via two TPP equation trees illustrated in Figure 1. The left tree computes the nominator of Equation 1: first the maximum value of the input tensor X is found (via the max-reduce TPP), then we subtract this max value from each entry of X (note the broadcast semantics in the second argument of the subtraction TPP), and a new tensor X' is computed by calculating the element-wise exponent on the earlier subtraction’s outcome. Finally, in the right TPP tree each entry of the tensor X' is normalized by the sum of all values in X' to obtain the softmax output, a tensor Y . This example illustrates the expressiveness of the TPP abstractions, since the components of the mathematical formula map to TPPs in a straightforward way. At the same time, this example highlights the separation of concerns: the user does not need to worry about the efficient implementation of this equation on each different platform, since the TPP back-end is responsible for optimized code generation which is target-specific (contrary to the TPP expression itself which is platform-agnostic).

4.2 Layernorm Kernel

Layer normalization (layernorm) [30] is a technique that normalizes the neurons *within* a layer, and was motivated by the limitations of Batch Normalization [31] in Recurrent Neural Networks. The layernorm computations can be divided in two stages: i) First the mean and variance of the input tensor are computed across the “feature” dimension: $\mu_i = \sum_{j=0}^{m-1} x_{ij}$, $\sigma_i^2 = \frac{1}{m} \sum_{j=0}^{m-1} (x_{ij} - \mu_i)^2$ where i is the batch dimension and j is the “feature” dimension, ii) then

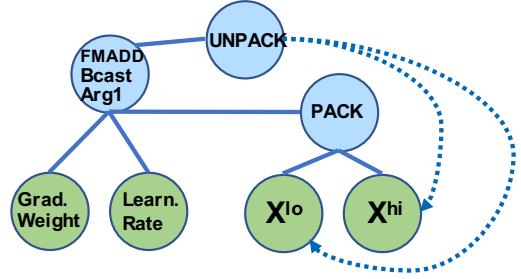


Figure 3: BF16 Split-SGD operator by combining TPPs.

the tensor entries x_{ij} are normalized based on μ and σ : $x'_{ij} = (x_{ij} - \mu_i) / (\sqrt{\sigma_i^2 + \epsilon})$. Depending on the workload (e.g. attention cell in BERT), the scaled tensor may be further scaled with two other tensors G and B . Figure 2 illustrates two TPP equation trees that implement this composite layernorm operator. The left equation is using the sum-reduce TPP to compute the sum and sum of squared elements of the input tensor, namely m and v . These two scalars are combined (not shown in the equation for simplicity), and are fed as inputs to the right TPP tree, where the FMADD ternary TPP is used to scale the input tensor X . Finally, a cascading FMADD ternary TPP computes the final result via the scaling tensors G and B . We illustrate this layernorm via means of TPPs since all DL norming layers essentially exhibit similar computational motif, and this specific norm is used in the BERT workload described in subsection 4.7.

4.3 BF16 Split-SGD Kernel

Unlike the two previous kernels which are well-established in DL workloads, and as such optimized in DL libraries, we present here an example of a novel operator, which per definition is not existent in DL libraries. BF16 split-SGD was recently introduced in the context of DLRM training with BF16 datatype [32]. The Split-SGD-BF16 solver aims at efficiently exploiting the aliasing of BF16 and FP32 (i.e. the 16 Most Significant Bits (MSB) on both are identical) in order to save bandwidth during the SGD-solver in training. The employed trick is that the weights are not stored as FP32 values in a single tensor. Instead, the FP32 tensors are split into their high and low 16bit-wide parts: the 16 MSBs of the FP32 values, and the 16 LSBs of the same values are stored as two separate tensors X^{hi} and X^{lo} respectively. The 16 MSBs represent a valid BF16 number and constitute the model/weight tensors during training. These BF16 weights are used exclusively in the forward and backward passes, whereas the lower 16 bits are only required in optimizer. More specifically, the X^{hi} and X^{lo} tensors are packed together to form an FP32 tensor, resulting in a fully FP32-accurate optimizer. Figure 3 illustrates the BF16 Split-SGD operator written entirely via TPPs. First the X^{hi} and X^{lo} are packed, and the formed FP32 tensor is used in a cascading FMADD TPP that performs the SGD scaling with the corresponding Gradient Weight tensor and learning rate. Finally, the resulting FP32 tensor is unpacked to the X^{hi} and X^{lo} tensors for further use in the training process.

Algorithm 3 1D Dilated convolution forward pass using TPPs

Inputs: $I^{C \times W}$, $W^{K \times C \times S}$, $d \in \mathbb{R}$

Output: $O^{K \times Q}$

```

1:  $W^T \leftarrow \text{TRANPOSE}(W)$ 
2: for  $pos = 0 \dots Q - 1$  with step  $b_q$  do
3:    $\triangleright$  Address-based BRGEMM, prepare arguments  $A_{ptrs}$ ,  $B_{ptrs}$ 
4:   for  $s = 0 \dots S - 1$  with step 1 do
5:      $A_{ptrs}[s] = \&W^T[s, 0, 0]$ 
6:      $B_{ptrs}[s] = \&I[0, (pos + s \cdot d)]$ 
7:    $\text{BRGEMM}(A_{ptrs}, B_{ptrs}, \&O[0, pos], S)$ 

```

4.4 Convolutional Neural Networks (CNN)

Convolutional Neural Networks (CNN) consist of layers with multiple neurons connected by weights, and they have been applied with success in image recognition, semantic segmentation, autonomous driving, medical imaging and in an increasing number of scientific applications. Previous work [21, 23] has shown that CNNs, despite their seemingly complicated loop structure due to the involved high-dimensional tensors, can be mapped efficiently onto small 2D GEMMs and BRGEMMs. In this work, we adopt the same strategy to implement CNNs via the BRGEMM TPP. Unlike the previous work which presents only the address-based BRGEMM formulation, here we leverage the CNN kernels with stride-based BRGEMM for 1×1 convolutions and offset-based BRGEMM for 3×3 convolutions to get even more performant implementations (see Section 2.2 for a brief description of the BRGEMM variants).

4.5 1D Dilated Convolutions & Comp. Bio

In this Section, we show the implementation of a special type of convolution via TPPs in their entirety, namely one-dimensional (1D) dilated convolution layer of a 1D CNN named ATACworks [33]. ATACworks is used for de-noising and peak calling from ATAC-Seq genomic sequencing data [33]. The 1D dilated convolution layer in ATACworks takes more than 90% of the training time, and it has input tensor width W , output tensor width Q , C input channels, K output channels, filter size of S , and dilation d . We employ the transpose TPPs, copy TPPs, and BRGEMM TPPs to optimize the forward pass and the backward pass of the PyTorch-based 1D convolution layer. Algorithm 3 shows an example of the forward pass procedure with an input tensor I , a weight tensor W , and an output tensor O .

4.6 Deep Learning Recommendation Model

Facebook recently proposed a deep learning recommendation model (DLRM) [34]. Its purpose is to assist the systematic hardware-software co-design for deep learning systems. DLRM comprises of the following major components: (a) a sparse embedding involving tables (databases) of varying sizes, (b) a small dense Multi-Layer Perceptron (MLP), and (c) a larger and deeper MLP which is fed by the interaction among (a) and (b). All three parts can be configured (number of features, mini-batch sizes and table sizes) to stress different aspects of the system. As such, we provide a high-level overview of how Sparse Embeddings and MLPs can be expressed via TPPs. For simplicity we focus on the forward propagation pass during



Figure 4: Sparse Embedding Lookups via TPPs

Algorithm 4 Fully-Connected Layer with Unary Activation Func.

Inputs: $A^{M_b \times K_b \times b_k \times b_m}$, $B^{N_b \times K_b \times b_n \times b_k}$

Output: $C^{N_b \times M_b \times b_n \times b_m}$

```

1: Based on thread_id calculate  $M_b\_start$ ,  $M_b\_end$ ,  $N_b\_start$  and  $N_b\_end$  to assign output work items
2: for  $ib_n = N_b\_start \dots N_b\_end$  do
3:   for  $ib_m = M_b\_start \dots M_b\_end$  do
4:      $Out = \&C[ib_n][ib_m][0][0]$ 
5:      $\triangleright$  Stride-based BRGEMM, stride_A =  $b_k \cdot b_m$ , stride_B =  $b_n \cdot b_k$ 
6:      $\text{BRGEMM}(\&A[ib_m][0][0][0], \&B[ib_n][0][0][0], Out, K_b)$ 
7:      $C[ib_n][ib_m][0][0] \leftarrow \text{UNARY}(C[ib_n][ib_m][0][0])$ 

```

training, however we have fully implemented the back-propagation in an analogous way by using solely TPPs. For more details on the workload and CPU-oriented optimizations we refer to prior work [32].

4.6.1 Sparse Embedding Kernel

The sparse embedding kernel is comprised of multi-hot encoded lookups into an embedding table $W^{M \times E}$ with M being the number of rows and E the length of each row, whereas the multi-hot weight-vector is denoted as $\alpha^T = [0, \dots, a_{p_1}, \dots, a_{p_k}, \dots, 0]$ with entries $a_p = 1$ for $p = p_1, \dots, p_k$ and 0 elsewhere (p being the index for the corresponding lookup items). Mathematically, the embedding lookup output vector o^T can be obtained via $o^T = \alpha^T \times W$. This operation (assuming row-major storage for W) is equivalent to gathering the rows of W based on the non-zero indices a_p , and then adding them up to get the output vector o^T . Figure 4 illustrates the TPP tree that is used to express the Sparse Embedding lookup kernel. We note that the TPP back-end optimizes this sequence of TPPs, and performs horizontal register fusion across them. More specifically, given a non-zero index a_p , the corresponding row of M is loaded in vector registers, and is added to a set of running accumulators/vector registers that hold the output o^T .

4.6.2 Multi-Layer Perceptron (MLP)

Multilayer perceptrons (MLP) form a class of feed-forward artificial neural networks. An MLP consists of (at least three) *fully connected* layers of neurons. Each neuron in the topology may be using a non-linear activation function. In this section we present the implementation of the *Fully Connected* layers since they constitute the cornerstone of MLP. Even though we illustrate the forward pass of Fully Connected layers, we also implement via TPPs the kernels of the back-propagation training in an analogous fashion. Algorithm 4 shows the fully connected layer implementation which is mapped to TPPs. First we note that the input tensors are conceptually 2D matrices $A^{M \times K}$ and $B^{K \times N}$ that need to be multiplied. We follow the approach of previous work [21] and we block the dimensions M , K , and N by factors b_m , b_k , and b_n respectively. Such a blocked layout is exposing better locality and avoids large,

strided sub-tensor accesses which are known to cause TLB misses and cache conflict misses in case the leading dimensions are large powers of 2 [21]. We leverage the BRGEMM TPP in order to perform the tensor contraction with A and B across their dimensions K_b and b_k (which constitute the K /inner-product dimension of the original 2D matrices). We employ the stride-based BRGEMM because the sub-blocks “ A_i ” and “ B_i ” that have to be multiplied and reduced are apart by constant strides $stride_A = b_k \cdot b_m$ and $stride_B = b_n \cdot b_k$ respectively. Finally, we apply (optionally) a unary TPP corresponding to the requested activation function (e.g. RELU) onto the just-computed output block of C .

4.6.3 BF16 Split-SGD optimizer

BF16 split-SGD, c.f. Section 4.3, was recently introduced in the context of DLRM training with BF16 datatype as an efficient way to implement the SGD optimizer [32].

4.7 Natural Language Processing - BERT

The BERT model is a bidirectional transformer; pre-trained via a combination of masked language modeling objective, and next-sentence prediction [35]. The heart of the BERT model is comprised by sequence of BERT layers which are built using smaller building blocks. For ease of use and implementation, we followed modular building blocks from Hugging Face transformers library [36] and implemented four fused layers using TPP building blocks, namely *Bert-Embeddings*, *Bert-SelfAttention*, *Bert-Output/Bert-SelfOutput* and *Bert-Intermediate* layers.

The *SelfAttention* layer in turn can be formulated as a bunch of of Matrix / batch Matrix-Multiplications mixed with element wise scale, add, dropout and softmax operator. We formulate these Matrix-Multiplications as tensor contractions on blocked-tensors via the stride-based BRGEMM TPP (similarly to Algorithm 4). We opt to use blocked tensor layouts for the same reasons briefly described in Section 4.6.2. Furthermore, by working on one small sub-tensor at a time we naturally follow a “dataflow” computation, which has been shown to maximize the out-of-cache-reuse of tensors among cascading operators [26, 37]. The softmax operator is also formulated entirely by TPPs as described in Section 4.1. We note that the sequence of Matrix-Multiplications in the attention layer requires sub-tensors to be transposed (and VNNI transformed in case of BF16 implementation), and for this task we leverage the transpose/transform TPPs. *Bert-Output* and *Bert-SelfOutput* layers perform GEMM over blocked layout, and fuse bias addition, dropout, residual addition and layernorm using TPPs. The *Bert-Embeddings* layer also performs layernorm and dropout after embedding lookups that are also implemented using TPPs. Finally, *Bert-Intermediate* layer performs blocked GEMM followed by bias addition and GELU activation function which we implement using the GELU TPP.

4.8 Emerging AI - Graph Neural Networks

Graph Neural Networks (GNN) [38] form an emerging class of Neural Network for learning the structure of large, population-scale graphs. Depending on the specific algorithm and task that a GNN is designed for (e.g. node classification, link prediction), feature-vector aggregation precedes or succeeds a shallow neural network. Such a neural network typically materializes one or more

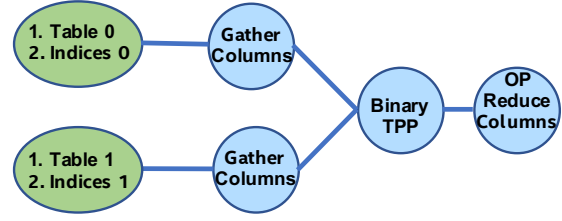


Figure 5: Binary-Reduce aggregation kernel via TPPs

linear transformations, followed by a classification or regression mechanism [39], and the relevant TPP-based implementation is essentially the one we present in Algorithm 4.

We focus here on the TPP-based implementation of the feature-vector aggregation. This aggregation motif can be seen as a sequence of linear algebraic expressions involving node/edge features, along with the appropriate operators. Prior work [39] has focused on the following two algebraic sequences: Copy-Reduce and Binary-Reduce. We elaborate here on the latter sequence Binary-Reduce (as the first is even simpler). The feature-vectors (either pertaining to vertices or edges) are represented via dense 2D matrices/tables. At the same time, the adjacency information in the graphs can be eventually found via arrays of indices. Therefore, by providing a set of indices and the appropriate Tables of feature-vectors (assuming column-major storage), one can extract selectively the desired feature-vectors via Gather-columns operations. Then, the extracted feature-vectors are fed into a binary operator, and the outcome of the binary operations are finally reduced (the reduce operation could be sum/max/min etc).

Figure 5 illustrates a TPP tree that is used to express the Binary-Reduce aggregation kernel. The TPP back-end optimizes this sequence of TPPs and performs horizontal register fusion across them. More precisely, two feature-vectors namely v_0 and v_1 are extracted at a time from Table 0 and Table 1 respectively, and they are combined via the proper binary op to get an intermediate output-vector v_i . Finally, v_i is reduced with a running reduce-vector that holds the output of this composite operator.

5 EXPERIMENTAL RESULTS

We use a variety of platforms that span different ISAs, different vendors and micro-architectures. More specifically, our tested platforms include: i) a 22-core Intel Xeon E5-2699 v4 (BDX) supporting up to AVX2 ISA, ii) a 28-core Intel Xeon 8280 (CLX) supporting up to AVX512 ISA, iii) a recently announced 40-core Intel Xeon 8380 (ICX) supporting also up to AVX512 ISA, iv) a 28-core Intel Xeon 8380H (CPX) supporting up to AVX512 ISA, which also offers BF16 FMA acceleration, v) a 64-core AMD EPYC 7742 (ROME) with AVX2 ISA, vi) an AWS Graviton2 instance with 64 cores at fixed 2.5 GHz and AArch64 ISA, and vii) a 48-core Fujitsu A64FX at fixed 1.8 GHz with ARMv8 SVE ISA. All Intel and AMD chips are operating in Turbo mode. For the cluster experiments we used a 32 node CLX installation with a dual-rail Intel Omnipath 100 pruned 2:1 fat-tree topology.

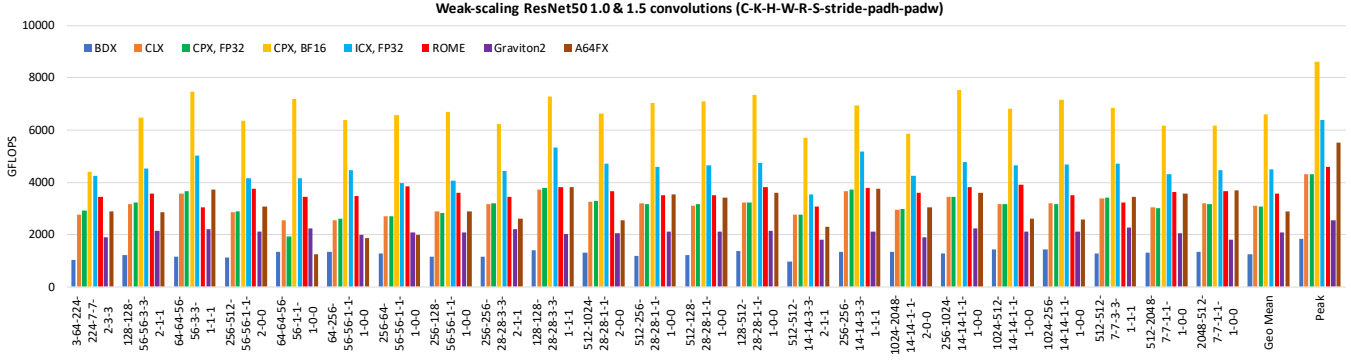


Figure 6: Convolutions via BRGEMM TPP

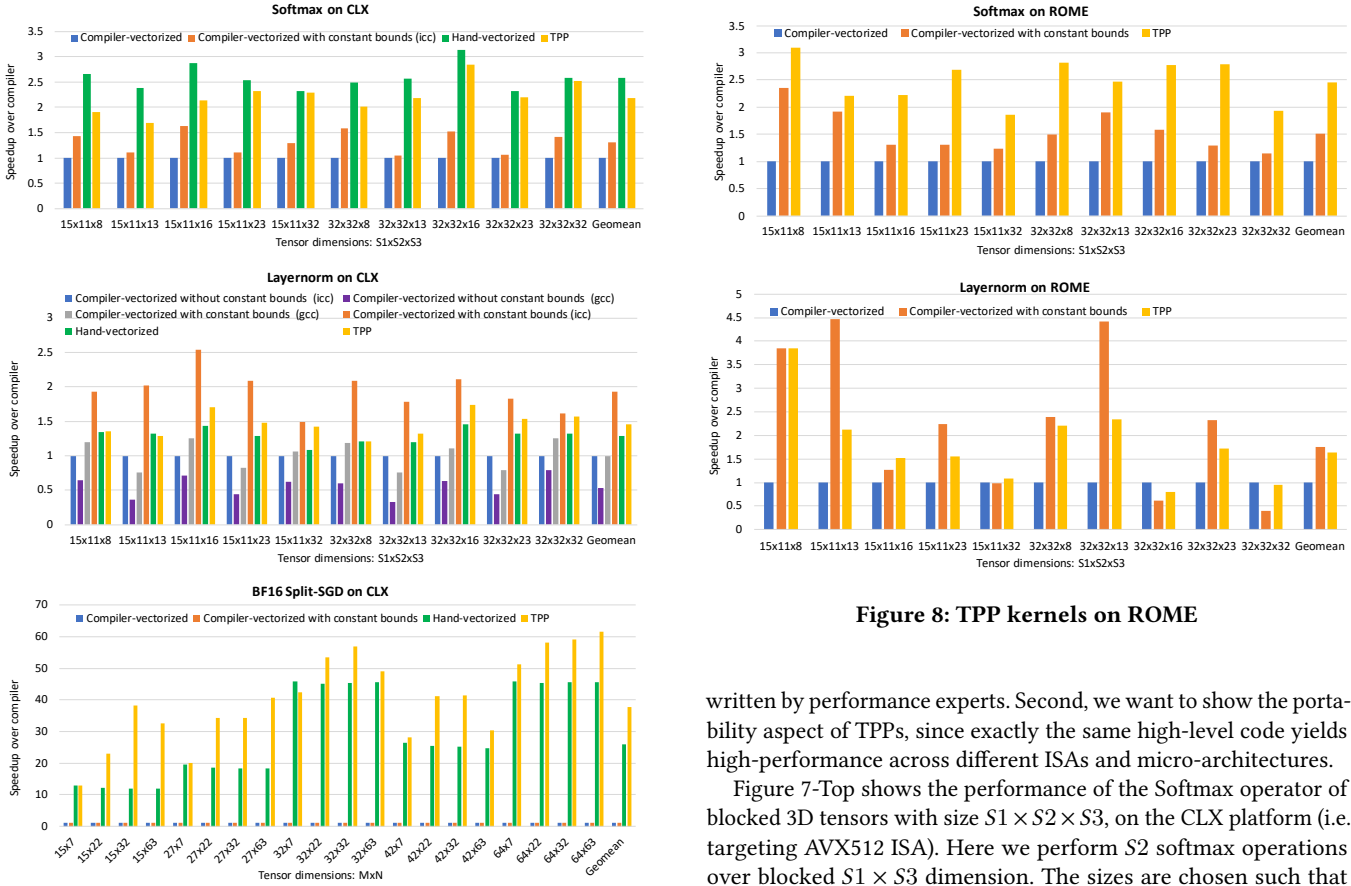


Figure 8: TPP kernels on ROME

Figure 7: TPP kernels on CLX

5.1 Performance of standalone DL kernels

We start the performance evaluation with the standalone TPP kernels presented in Sections 4.1, 4.2, and 4.3. First, we want to highlight the productivity/efficiency provided by TPPs: the high-level code expressed via TPPs/trees of TPPs can match or outperform code by compilers, and hand-vectorized (thus non-portable code)

written by performance experts. Second, we want to show the portability aspect of TPPs, since exactly the same high-level code yields high-performance across different ISAs and micro-architectures.

Figure 7-Top shows the performance of the Softmax operator of blocked 3D tensors with size $S1 \times S2 \times S3$, on the CLX platform (i.e. targeting AVX512 ISA). Here we perform $S2$ softmax operations over blocked $S1 \times S3$ dimension. The sizes are chosen such that some of the dims do not match perfectly with the vector length. The baseline is the icc generated code with `-O3` optimization level `high-zmm` usage. The second variant is also icc-generated code, but we propagate the tensor sizes/loop bounds via compile-time constants in order to assist the auto-vectorization/optimize remainder handling via masking. The third code variant is the AVX512 hand-vectorized by an expert, where the `exp` function uses fast Taylor approximation. Last, we evaluated the TPP-based softmax implementation. As we can see, by propagating the tensor sizes we achieve (geo-mean) speedup of 1.3 \times over the baseline. The hand-vectorized code is faster by 2.6 \times whereas the TPP-based variant

shows similar speedups by being 2.2 \times faster. The main shortcoming of the hand-vectorized code is that it is platform-dependent and as such non-portable. More specifically, we didn't have to our avail AVX2 hand-optimized code in order to experiment with it on ROME. On the contrary, Figure 8-Top shows the softmax performance on AVX2 enabled platform for the compiler-generated code and the TPP based code. The TPP-based softmax exhibits geo-mean speedup of 2.45 \times over the baseline on ROME.

Figure 7-Middle shows the performance of the layernorm operator on the CLX platform. Since the layernorm code is more straightforward (i.e. no expensive *exp* function is involved), we see that icc with compile-constant bounds outperforms by 1.9 \times the baseline. We inspected the compiler-generated code and identified that the reduction-loops were recognized and were heavily optimized with multiple accumulation chains etc. Similarly, the hand-vectorized code and the TPP based code outperform the baseline by 1.3 \times and 1.5 \times . We also experimented with gcc and the *fast-math* flag, and it just matched baseline performance. We want to emphasize that propagating the tensor sizes as compile-time constants throughout the operators is not practical for real use-cases within DL frameworks. Figure 8-Bottom shows similar performance speedups on ROME, where the TPP-based code is 1.6 \times faster than the auto-vectorized baseline.

Figure 7-Bottom shows the performance of the BF16 split-SGD operator on CLX. This use-case represents a novel, mixed-precision operator where the compiler (even with compile-time constant tensor sizes) struggles to yield good performance; the TPP-based code has geo-mean speedup of 38 \times over the compiler generated code.

Figure 6 illustrates the TPP-based implementation of various ResNet50 [40] Convolution layers across all available platforms. The minibatch size used on each platform equals to the number of the corresponding cores. It is noteworthy that the TPP-user code is identical for all targets, hence truly portable; it is merely that the TPP backend optimizes the code generation (BRGEMM in this case) in a platform/ISA-aware fashion. The geomean efficiencies of these convolutions are: 69% for BDX, 72% for CLX, 72% for CPX, 77% for CPX with BF16 datatype, 70% for ICX, 78% for ROME, 81% for Graviton2 and 52% for A64FX. Previous work [21] also showed on an x86 TPP-predecessor that BRGEMM-based convolutions matched or outperformed Intel's oneDNN library [13]. Fujitsu recently contributed a A64FX backend to oneDNN [41] and our TPP implementation outperforms this by 22% on the geomean. We observe that our TPP convolutions not only run on all of these different platforms without a single line of code change, but they run at very similar hardware utilization, the hardest and strictest definition of performance portability.

5.2 Performance of end-to-end DL workloads

5.2.1 1D Dilated Convolutions and their application to Comp. Bio

Here we evaluate the oneDNN [13] and TPP-based 1D dilated convolution layer of ATACworks [33] which takes takes more than 90% of the training time, and it has input tensor width (W) of 60400, output tensor width (Q) of 60000, 15 input channels (C), 15 filters (K), filter size (S) of 51, and dilation (d) of 8. Figure 9-Top shows the computational efficiency results of the 1D convolution layer.

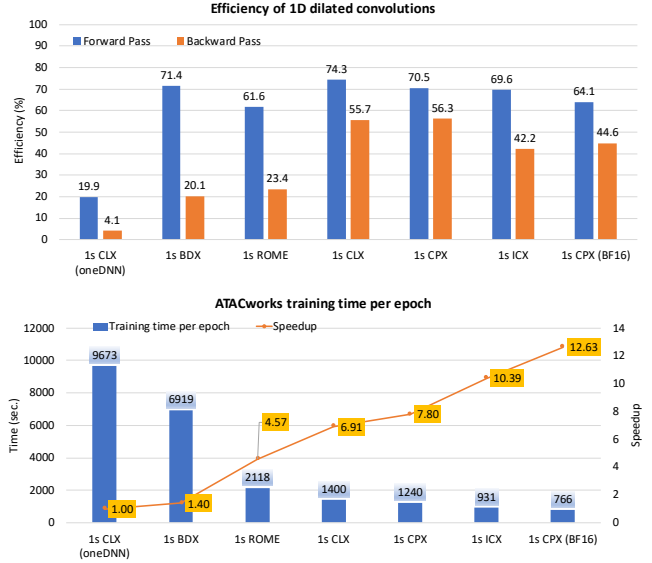


Figure 9: 1D Dilated Convolutions

oneDNN is not reaching peak for this specialized convolutions, exhibiting 19.9% efficiency for the forward pass and only 4.1% for the backward pass on CLX. Our TPP-based implementation shows 74.3% and 55.7% efficiency for the corresponding training passes. We also highlight the performance portability of our TPP-based approach across all tested platforms. Finally, we show training time per epoch results for ATACworks in Figure 9-Bottom. The TPP-based kernels provide training time speedup of 6.91 \times on CLX when comparing to the oneDNN based implementation. We also show that by leveraging the BF16 FMA acceleration of the CPX platform we can further obtain 1.62 \times speedup compared to the FP32 implementation on the same platform. In total BF16 yields 12.6 \times speedup over the oneDNN baseline.

5.2.2 Deep Learning Recommendation - DLRM

Figure 10-Top shows the FP32 DLRM performance on CLX using two different configurations, namely small DLRM and MLPerf DLRM configurations. We refer to previous work for the detailed specification of these configurations [32]. We evaluated 4 different implementations of DLRM: i) the PyTorch reference implementation, ii) PyTorch reference + custom Embedding extension auto-vectorized by the compiler, iii) DLRM expressed entirely via TPPs, and iv) hand-vectorized Embedding extension + BRGEMM based MLPs [32]. We conclude that the TPP-based implementation matches the performance of the State-Of-The-Art implementation which is hand-vectorized specifically for AVX512 targets; both of these optimized versions substantially outperform the PyTorch CPU reference implementation by up to 49 \times . Compared to the version with the custom, auto-vectorized variant the TPP-version is up to 4.4% faster.

Figure 10-Bottom shows the DLRM performance of our TPP-based implementation across multiple platforms and compute precisions. We want to highlight two aspects: First, we are able to run the same TPP-code without any change across all platforms, something that is not doable with the hand-vectorized SOTA variant (iv)

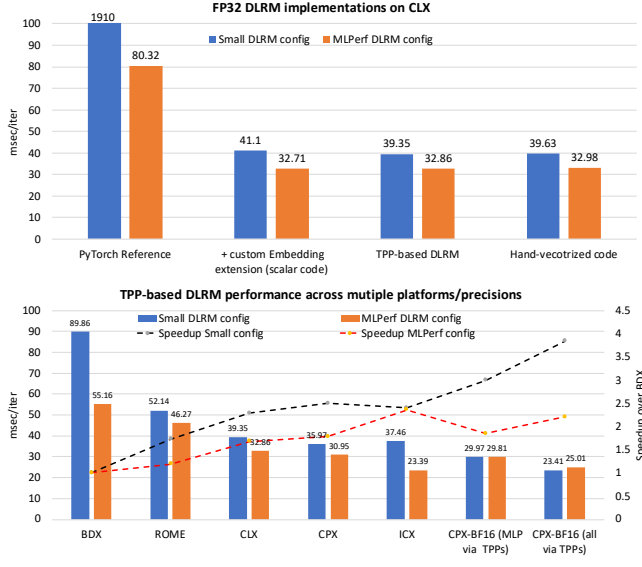


Figure 10: DLRM performance

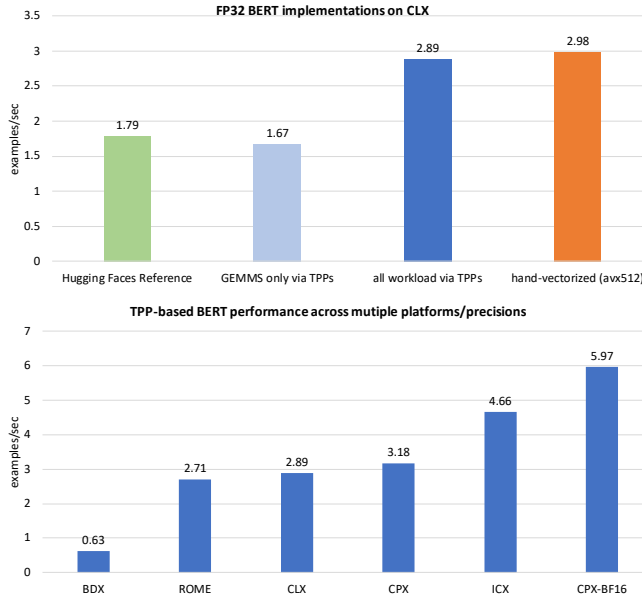


Figure 11: BERT Large performance

(since it is not able to run on the AVX2-only BDX and ROME platforms). Second, the TPP-based BF16 shows speedup up to 28% over the variant with auto-vectorized Embedding extension. The culprit here is the mixed precision operations like split-SGD where the compiler struggles to yield efficient code as shown in Section 5.1.

5.2.3 Natural Language Processing - BERT Large

Figure 11-Top shows end-to-end performance (in examples/second) on CLX for the BERT large SQuAD fine-tuning task in FP32, using a max sequence length of 384 and minibatch of 24. We observe that the TPP-based implementation matches the performance of

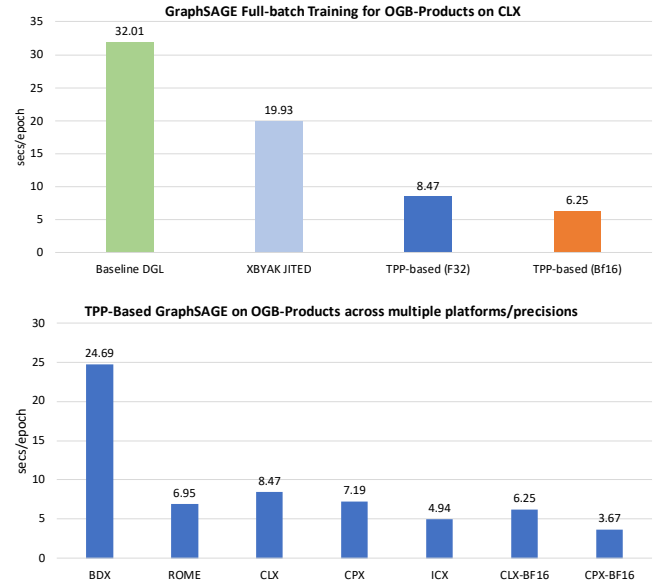


Figure 12: GNN performance

the AVX512-hand-vectorized code (within 3%). At the same time, our implementation is 1.61 \times faster than the Reference HuggingFace CPU reference code [42]. Figure 11-Bottom shows the performance of the TPP-based code across multiple platforms and compute precisions. The relative differences in the performance can be justified by the different compute/bandwidth specs of the benchmarked platforms. It is noteworthy to mention that with minimal changes inside the fused operators to handle VNNI layout required for BF16 GEMM, and couple of lines change in application code to enable BF16 training, we were able to realize 1.8 \times speed up using BF16 training on CPX with 28 cores surpassing 40 core ICX performance by 30%.

5.2.4 Emerging AI - Graph Neural Networks

Figure 12-Top shows end-to-end performance (in seconds/epoch, so lower is better) on CLX for the full-batch training of the GraphSAGE workload on OGB-Products with FP32 and BF16 precision; for the CLX BF16 experiments, since CLX doesn't have native support for BF16 FMAs, we use bit-wise accurate emulated-BF16 BRGEMM TPPs, and we still expect savings due to the bandwidth saving in the non-GEMM parts, e.g., graph traversal and edge/node aggregation. We observe that the TPP-based implementation outperforms the DGL [43] baseline by 3.8 \times and the Xbyak JITed/optimized version (non-default optimization in DGL) by 2.35 \times . TPP-BF16 yields another 1.33 \times speedup over the TPP-FP32 mainly due to bandwidth.

Figure 12-Bottom shows the performance of the TPP-based code across multiple platforms and compute precisions. The relative differences in the performance can be justified by the different compute/bandwidth specs of the benchmarked platforms. We highlight that with minimal changes in the MLP portion to handle VNNI layout required for BF16 BRGEMM, and couple of lines change in application code to enable BF16 training, we were able to realize 1.96 \times speed up using BF16 training on CPX with 28 cores compared to the FP32 training on the same platform.

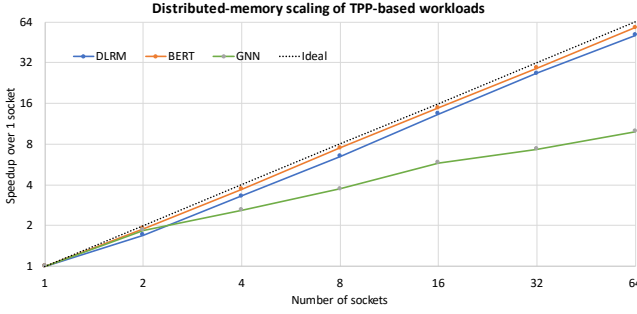


Figure 13: Distributed-memory scaling of workloads

5.3 Distributed-memory scaling of workloads

Even though we focused on the evaluation of the TPP-based workloads on a single node, our approach is seamlessly incorporated into the DL frameworks, hence we can scale to multiple nodes in a cluster to accelerate the training process employing the oneCCL library [44]. Figure 13 shows the distributed-memory scaling of the TPP-based workloads. DLRM and BERT show almost perfect weak-scaling from 1 to 64 sockets of CLX (32 nodes) with speedups 51.7 \times and 57.9 \times respectively. Regarding the scaling of the GNN workload, the efficiency is directly affected by the quality of the partitions produced by the graph partitioning tools. Using 64 sockets we achieve 10 \times speedup compared to single socket, and further scaling improvements constitute future work. We can conclude that TPPs for single node optimizations combined with small-size cluster level execution can accelerate deep learning training on CPUs by up to two orders of magnitude.

6 HPC IMPLICATIONS & RELATED WORK

While the presentation in this work focused on how TPPs can be used to express DL computations in a performance portable way across various architectures and precisions, TPPs can be of course applied in HPC as well. Especially quantum chemistry (CP2K [45]) and higher finite element solvers (pyFR [46], EDGE [47], Nek* [48], SeisSol [49], Spectre [50] and libCEED [51]) make already heavy use of the versatile (BR)GEMM TPP. An extension to the element-wise TPPs and hence even increasing performance portability in this expanded application field is straightforward.

The related work in terms of the development methodology of DL workloads has been referenced in the introduction, so here we mention community efforts that share the same design philosophy with TPPs. Tensor Operator Set Architecture (TOSA) is a recent work, concurrently developed with TPPs, that provides a set of whole-tensor operations commonly employed in DL [52]. TOSA allows users to express directly operators on up to 4D/5D tensors which are not naturally mapped even on contemporary 2D systolic hardware. We believe that staying at the 2D primitive level is expressive and sufficient, as we can build higher-order ops with loops around 2D operators, e.g. see Algorithm 4. Despite the similarities of TPP and TOSA specifications, the TOSA back-end is reference C code and is not showcased in full DL-workloads. CUTLASS [53] and Triton [54] strive for high-performance on GPUs, while also offering flexible composition that can be easily applied to solve new

problems related in DL and linear algebra, and share many design principles with TPPs. XLA [55] is a domain-specific compiler for linear algebra and DL that targets TensorFlow models with potentially no source code changes. JAX [56] provides automatic differentiation of Python and NumPy functions, and the compilation of the desired operators happens in a user-transparent way with JIT calls, yielding optimized XLA kernels. XLA and JAX share the same philosophy with TPPs: the user is focusing on the DL kernel/workload development using high-level, platform-agnostic, declarative-style programming, whereas the tensor-aware back-end infrastructure undertakes the efficient, and portable code generation.

Tensor Compilers (TC) [15–18] attempt to optimize DL operators in a platform-agnostic way, however their applicability is restricted to relatively small code-blocks whereas full workload integration is cumbersome. Also, TC undertake the tasks of efficient parallelization, loop re-orderings, automatic tiling and layout transformations, nevertheless the obtained performance is typically underwhelming [12]. We envision that TPPs can be used as a tool by TC in order to attain efficient platform-specific code generation, therefore TC could focus on optimizing the higher level aspects of the tensor programs (e.g. layout transformations). Along these lines, TPPs fit in the MLIR [20] ecosystem/stack as a lowering dialect, and in this way the TPP back-end could be leveraged by multiple TC frameworks.

7 CONCLUSIONS AND FUTURE WORK

In this work we presented the Tensor Processing Primitives (TPP), a compact, yet versatile set of 2D-tensor operators, which subsequently can be utilized as building-blocks to construct efficient, portable complex DL operators on high-dimensional tensors. We demonstrate the efficacy of our approach using standalone kernels and end-to-end training DL-workloads (CNNs, dilated convolutions, DLRM, BERT, GNNs) expressed entirely via TPPs that outperform state-of-the-art implementations on multiple platforms. As future work, we plan to create a TPP-based MLIR dialect such that Tensor Compilers can leverage the strengths of TPPs. Also, we plan to further enrich the TPP back-end implementation by supporting more ISAs, including GPUs and POWER architectures.

REFERENCES

- [1] Alex Krizhevsky, I. Sutskever, and G.E. Hinton. Image classification with deep convolutional neural networks. *Advances in neural information processing systems*, pages 1097–1105, 2012.
- [2] Christian Szegedy, Wei Liu, Yangqing Jia, Pierre Sermanet, Scott Reed, Dragomir Anguelov, Dumitru Erhan, Vincent Vanhoucke, and Andrew Rabinovich. Going deeper with convolutions. In *Proceedings of the IEEE conference on computer vision and pattern recognition*, pages 1–9, 2015.
- [3] Karen Simonyan and Andrew Zisserman. Very deep convolutional networks for large-scale image recognition. *arXiv preprint arXiv:1409.1556*, 2014.
- [4] Dong Yu, Michael L Seltzer, Jinyu Li, Jui-Ting Huang, and Frank Seide. Feature learning in deep neural networks-studies on speech recognition tasks. *arXiv preprint arXiv:1301.3605*, 2013.
- [5] Yonghui Wu, Mike Schuster, Zhifeng Chen, Quoc V Le, Mohammad Norouzi, Wolfgang Macherey, Maxim Krikun, Yuan Cao, Qin Gao, Klaus Macherey, et al. Google’s neural machine translation system: Bridging the gap between human and machine translation. *arXiv preprint arXiv:1609.08144*, 2016.
- [6] Heng-Tze Cheng, Levent Koc, Jeremiah Harmsen, Tal Shaked, Tushar Chandrasekhar, Hrishikesh Aradhye, Glen Anderson, Greg Corrado, Wei Chai, Mustafa Ispir, et al. Wide & deep learning for recommender systems. In *Proceedings of the 1st Workshop on Deep Learning for Recommender Systems*, pages 7–10. ACM, 2016.
- [7] Thomas Wolf, Julien Chaumond, Lysandre Debut, Victor Sanh, Clement Delangue, Anthony Moi, Pierric Cistac, Morgan Funtowicz, Joe Davison, Sam Shleifer, et al.

[31] Sergey Ioffe and Christian Szegedy. Batch normalization: Accelerating deep network training by reducing internal covariate shift. In *International conference*

and Tom Włodarczyk. Spectre, April 2021.

- [51] Ahmad Abdelfattah, Valeria Barra, Natalie Beams, Jed Brown, Jean-Sylvain Camier, Veselin Dobrev, Yohann Dudouit, Leila Ghaffari, Tzanio Kolev, David Medina, Thilina Rathnayake, Jeremy L. Thompson, and Stanimire Tomov. libceed user manual, September 2020.
- [52] TOSA. <https://developer.mlplatform.org/w/tosa/>, Accessed on 3/30/2021.
- [53] NVIDIA CUTLASS. <https://github.com/nvidia/cutlass>, Accessed on 3/30/2021.
- [54] Philippe Tillet, HT Kung, and David Cox. Triton: an intermediate language and compiler for tiled neural network computations. In *Proceedings of the 3rd ACM SIGPLAN International Workshop on Machine Learning and Programming Languages*, pages 10–19, 2019.
- [55] XLA: Optimizing Compiler for Machine Learning. <https://www.tensorflow.org/xla>, Accessed on 3/30/2021.
- [56] JAX: Autograd and XLA. <https://github.com/google/jax>, Accessed on 3/30/2021. Optimization Notice: Software and workloads used in performance tests may have been optimized for performance only on Intel microprocessors. Performance tests, such as SYSmark and MobileMark, are measured using specific computer systems, components, software, operations and functions. Any change to any of those factors may cause the results to vary. You should consult other information and performance tests to assist you in fully evaluating your contemplated purchases, including the performance of that product when combined with other products. For more information go to <http://www.intel.com/performance>. Intel, Xeon, and Intel Xeon Phi are trademarks of Intel Corporation in the U.S. and/or other countries.